Journal of
Marine Science and Engineering

MDPI

Article

Short-Term/Range Extreme-Value Probability Distributions of Upper Bounded Space-Time Maximum Ocean Waves

Alvise Benetazzo *, Francesco Barbariol and Silvio Davison

Istituto di Scienze Marine (ISMAR), Consiglio Nazionale delle Ricerche (CNR), 30122 Venice, Italy; francesco.barbariol@ve.ismar.cnr.it (F.B.); silvio.davison@ve.ismar.cnr.it (S.D.)

* Correspondence: alvise.benetazzo@ismar.cnr.it

Received: 4 August 2020; Accepted: 2 September 2020; Published: 3 September 2020

Abstract: There is general consensus that accurate model predictions of extreme wave events during marine storms can substantially contribute to avoiding or minimizing human losses and material damage. Reliable wave forecasts and hindcasts, together with statistical analysis of extreme conditions, are then of utmost importance for monitoring marine areas. In this study, we perform an analysis of the limitations of the available short-term/range extreme-value distributions suitable for space-time maximum wave and crest heights. In particular, we propose an improvement of the theoretical distributions by including upper bounds on the maximum heights that waves may reach. The modification of the space-time probability distributions and its impact for extreme-value assessment is discussed in the paper. We show that unbounded space-time distributions are still effective provided that the surface area included in the analysis has sides smaller than $O(10^2$ m). For wider surfaces, the use of the bounded distributions is consistent with the expected saturation of maximum heights that ocean waves attain.

Keywords: ocean wave extremes; space-time maximum crest and wave heights; rogue waves

1. Introduction

The characterization of maximum wind-wave heights during marine storms has been an active topic of research for decades because of its importance for marine safety, coastal hazards, offshore design and operations. Significant efforts have been undertaken to better understand the likelihood and amplitude of extreme events, including rogue and freak waves [1–14]. Present strategies, however, resulted sometimes ineffective in warning seafarers or avoiding structural damage to offshore facilities (see e.g., [6,15,16]). Theoretical progress has been accompanied by numerical model improvements, so that currently most of the state-of-the art phase-averaged wave models, used for forecast and hindcast numerical studies, are equipped with routines that provide estimates of wave extremes (namely maximum crest height and maximum wave height) during storms [17–20].

The condition that supports the estimate of extreme sea waves is the steady-state (in time t) and homogenous (on the two-dimensional xy-space) sea condition, and the derived statistics is referred to as short-term/range (time interval from minutes to 1 h or so and spatial distance up to a thousand meters). In the temporal domain t only, the short-term extremal probability pertains to sea surface elevation $\eta(t)$ time series at a fixed point $\boldsymbol{x}_0 = (x_0, y_0)$ on the water surface, where x and y are the two Cartesian horizontal axes. Starting from the Rayleigh distribution [21], it has been established that nonlinear second-order bound waves and four-wave nonlinear interactions have a profound impact on the statistics of extreme events over $\eta(t)$ [2,12,22,23]. More recently, following the works of Adler [24] and Piterbarg [25] for multidimensional manifolds, the concept of excursion probability was introduced

and the time statistics was extended to the two-dimensional xy-space [26–29] by incorporating the short-range condition for the space-time surface elevation field $\eta(x, y, t)$.

For long time intervals and large sea surface areas, both time and space-time extreme theoretical models, being based on Gaussianity (or weakly nonlinear Gaussian seas) and constructive interference, never reach saturation, thus leading to overestimation of maximum surface heights. This implies that there are no physical limits on the values that the surface height can attain as the Gaussian model does not account for the saturation induced by the nonlinear dispersion [30] or wave breaking [31]. This limitation is more pronounced for space-time extremes with large sample size (namely over a wide area A or a long-time interval D, or a combination of the two) that therefore may provide unrealistically high amplitudes. The above-mentioned overestimation is a well-known feature of extreme-value analyses that incorporate a spatial contribution [6] and indeed their applications were wisely limited to assessments over sea areas with a size of a few hundreds of meters, where theoretical models proved to be valuable [28,32–36].

In this study, we propose a modification, suitable for being used even for large areas, of the short-term/range extreme-value probability distributions of (*i*) maximum crest heights, after Benetazzo et al.'s [32] formula based on the Adler's model of the Euler characteristics [26,29] and Tayfun nonlinear correction [37], and (*ii*) maximum crest-to-trough wave heights [38] which stems from the Quasi-Determinism (QD) asymptotic theory by Boccotti [39]. This aim is achieved by imposing upper heights that maximum waves cannot exceed given a characteristic scale of the sea state. The basic principles, capability, and weakness of our assumptions, as well as their impact on space-time extreme assessments are considered in this study. Our purpose is to extend the application of space-time wave extremes by imposing an additional physical constraint that allows more realistic probability distributions and expected values of the random variables to be determined.

The paper will proceed as follows. Section 2 is dedicated to explaining the bounded and unbounded theoretical formulations for spatio-temporal maximum crest and wave heights. Section 3 presents the assessment of the bounded distribution against data available in the literature. The impact of the bounded distribution on space-time extreme waves is examined in Section 4. A discussion and summary of the main conclusions of the study are presented in Section 5.

2. Short-Term/Range Statistics of Extreme Waves

2.1. The Extreme-Value Distribution of the Spatio-Temporal Maximum Crest and Wave Heights

The short-term/range excursion probability $\Pr\{\cdot\}$ of second-order nonlinear maximum crest heights C_m belonging to wave groups crossing a two-dimensional sea surface area $A = XY$ (X and Y are the area sides along the two orthogonal directions x and y, respectively) and time duration D was here approximated after Adler [40], and following Fedele [26], Baxevani and Rychlik [29] and Benetazzo et al. [32] as follows

$$\Pr\{C_m \geq \sigma h \mid DA\} \approx \left[N_3\left(h_0^2 - 1\right) + N_2 h_0 + N_1\right] \exp\left(-\frac{h_0^2}{2}\right) \tag{1}$$

where the elevation threshold h is normalized with the standard deviation σ of the sea surface elevation field $\eta(x, y, t)$, and

$$h_0 = \left(-1 + \sqrt{1 + 2\mu h}\right)\mu^{-1} \tag{2}$$

is the solution of the Tayfun equation [37] that relates the second-order nonlinear dimensionless threshold (h) to its linear counterpart (h_0) via the steepness parameter $\mu > 0$ [23]. In Equation (1), N_3 is the average number of waves within the space-time region Γ of three-dimensional volume $V = XYD$, N_2 is the average number of waves on the two-dimensional faces of Γ, and N_1 is the average number of waves on the one-dimensional edges of Γ. These numbers of waves depend on the spectral moments

through the definition of the mean zero-crossing period, the mean zero-crossing wave length, the mean wave crest length, and a measure of the irregularity of the space-time sea surface elevation field [26,38].

Assuming the excursion probability in Equation (1) is continuous, its asymptotic Gumbel limit for high values of h is easily found to have a cumulative distribution function (cdf) as follows [26]:

$$F_{\mathrm{Cm}}(h) \;=\; \mathrm{P}(C_{\mathrm{m}} \le \sigma h \,|\, DA) \approx\; \exp[-\exp(-z)] \tag{3}$$

where P represents the probability that the random variable C_{m} takes on a value less than or equal to σh. The Gumbel variable z (that incorporates location and scale parameters) is written as

$$z \;=\; \frac{\left(h-\xi_0-\frac{\mu}{2}\xi_0^2\right)\left(\xi_0-\frac{2N_3\xi_0+N_2}{N_3\xi_0^2+N_2\xi_0+N_1}\right)}{1+\mu\xi_0} \tag{4}$$

and ξ_0 is the dimensionless mode of the linear part of the extremal probability in Equation (1). By differentiating, the probability density function (pdf) of the Gumbel distribution of the random variable C_{m} is given by

$$f_{\mathrm{Cm}}(h) = \mathrm{d}F_{\mathrm{Cm}}(h)/\mathrm{d}h \tag{5}$$

and the expected value of C_{m} is calculated as follows

$$\mathrm{E}\{C_{\mathrm{m}}\} = \;\sigma\int_0^{\infty} h f_{\mathrm{Cm}}\mathrm{d}h \tag{6}$$

where $\mathrm{E}\{\cdot\}$ denotes expectation. In summary, the extreme-value statistical model based on the Adler approach and the Tayfun theory allows finding a short-term/range extreme-value statistics for second-order weakly nonlinear crest heights C_{m} belonging to space-time wave groups.

Unlike C_{m} or in the temporal domain [39,41], in the two-dimensional spatial and three-dimensional spatio-temporal domain, an analogous distribution for maximum crest-to-trough wave height H_{m} does not have a closed-form solution [26,35], given that the generalization to high-dimension excursion sets of the notion of wave profile, from which to infer the crest-to-trough vertical distance, is ambiguous. Notwithstanding, we have used the linear QD model by assuming it as to be effective for each realization of a space-time wave group holding maximum waves. In this case, by imposing $\mu = 0$, the Gumbel variable in Equation (4) loses its nonlinear part (therefore $h = h_0$) and z simplifies to [26]

$$z_0 \;=\; (h-\xi_0)\left(\xi_0-\frac{2N_3\xi_0+N_2}{N_3\xi_0^2+N_2\xi_0+N_1}\right) \tag{7}$$

The Gumbel-like cumulative distribution function for space-time linear maximum crest heights can be then approximated as

$$F\mathrm{Cm}_0(h) \;=\; \mathrm{P}(C_{\mathrm{m}0} \le \sigma h \,|\, DA) \approx\; \exp[-\exp(-z_0)] \tag{8}$$

where "0" in the subscripts indicates linear theory prediction. The pdf of $C_{\mathrm{m}0}$ can be analytically inferred by derivation as follows

$$f_{\mathrm{Cm}0}(h) = \mathrm{d}F_{\mathrm{Cm}0}(h)/\mathrm{d}h \tag{9}$$

We then made use of the linear QD theory by imposing a change of variable of the type $H = \alpha h$, where the coefficient $\alpha = \sqrt{2(1-\psi^*)}$ was purposely used to relate the maximum crest and wave heights in sea states with finite bandwidth, which is specified by the first minimum $\psi^* \in [-1,\, 0)$ of the sea surface elevation autocovariance function [39]. The pdf of maximum wave heights H_{m} was thus obtained from that of maximum crest heights as follows

$$f_{\mathrm{Hm}}(H) = \alpha^{-1} f_{\mathrm{Cm}0}(h) \tag{10}$$

The expectation of the random variable H_m is given by

$$\mathrm{E}\{H_m\} = \sigma \int_0^\infty H f_{Hm} \mathrm{d}H \tag{11}$$

It is worth noting that this result is consistent with the prediction of the QD theory that yields an equality for mean quantities, i.e., $\mathrm{E}\{H_m\} = \alpha \mathrm{E}\{C_m\}$, as corollary of the relationship that exists between the space-time wave group of the maximum expected crest height and the wave group of the maximum expected crest-to-trough height. To complete this section, we recall, and it was used in the following analyses, that all parameters of the extreme-value probability distributions may be obtained using higher-order moments of the directional wave spectrum [26].

2.2. Extreme-Value Distribution of Upper Bounded Maximum Heights

As we reported earlier, the pdf of unbounded space-time extremes, being based on Gaussianity, has no physical limits on the values that the surface height or crest-to-trough height can attain. In practice, zero-probability events, which are events whose probability is zero, are not allowed. This is far from being realistic, since many physical processes govern the scale of wave growth. One of the important processes driving the wind-wave evolution is the energy dissipation via breaking [31]. When breaking occurs, it produces a sudden reduction of wave height and consequently wave energy; it was estimated that a breaking wave may lose more than half of its height [42] in a space less than one wavelength [43]. Over a surface area, breaking appears randomly and the fraction of breaking waves is such that, on average, every 20th to 50th wave displays breaking [31], a fact that would favor the likelihood of encountering a breaking wave as the area increases. During the breaking onset, waves approach an instability condition that ultimately reduces their height, whether waves relax back or steepen further and collapse. After Stokes [44], the most common criterion for wave breaking in deep water employs the local steepness, by limiting the height-to-wavelength ratio H/L. This geometric criterion, originally thought for linear monochromatic waves, was confirmed as the limit for wave breaking induced by linear wave focusing [45], and for breaking due to modulation instability [46]. Further, local effects, such as the superimposed wind forcing [47] or the ocean surface current gradients [48], may influence the formation of breaking, steep waves.

The parameterization of the ultimate steepness beyond which directional waves will certainly break, and the pdf of wave steepness H/L has a sudden cut-off, is not straightforward in the context of extreme-value theories. There are two main limitations. First of all, theoretical criteria based on the maximum steepness appear rather as upper bounds, even when they are converted into equivalent formulations for nonlinear crest heights [49]. Indeed, measurements from laboratory [50] and field experiments [51] suggested that waves generally break below the Stokes limiting steepness. Secondly, those criteria require the knowledge of the local wave-by-wave length L [52] from which one can infer the maximum wave steepness H_m/L (or C_m/L). However, since parameters of the extreme height pdf are computed from the wave spectrum, the deterministic value of the local L for each realization of maximum waves is unknown; indeed, amplitudes and therefore steepness of waves with a specific wavenumber are not deterministically defined in the continuous-spectrum environment [31], so that a probabilistic approach was established [53,54]. This makes the computation of the individual steepness and the simulation of breaking an unviable solution to judge whether or not an individual maximum wave of a given height is breaking. We have therefore decided to give up the search of a limiting steepness, and we have loosely used normalized (with the significant wave height $H_s = 4\sigma$) limiting crest and crest-to-trough heights for the maximum waves. In the following, we show how the extreme-value pdfs are modified to account for such a maximum value, while in the next section we discussed how to characterize maximum allowable heights, and we assessed the theoretical formulation against literature data.

From a statistical point of view, we aimed at restricting the unbounded sample space $(0, \infty)$ of the two density functions f_{Cm} and f_{Hm} by equalling them to zero above a finite height threshold; in other words, we wish to know the probability density of the non-negative random variables C_{m} and H_{m}, after limiting the corresponding support to be below a threshold scaled with H_{s}. We proceed by assuming that (*i*) before reaching the threshold, maximum waves are allowed to grow and decay and the random process and its extreme-value probability distribution are unaffected, and (*ii*) the upper bound is an accumulation point for the extreme-value statistics. This is a further simplification of the effects of wave breaking, since it forces the height reduction after breaking, by assigning a normalized height that maximum waves cannot exceed. This choice is however reasonable since we are taking into account the extreme-value pdf of maximum heights, which describe the distribution of maximum parameters over an ensemble of realizations.

Accordingly, we might first write the condition for maximum crest heights C_{m} as follows

$$g_{\mathrm{Cm}}(h; B_{\mathrm{c}}) = \ f_{\mathrm{Cm}}(h \mid 0 < C_{\mathrm{m}} \leq B_{\mathrm{c}} H_{\mathrm{s}}) \tag{12}$$

by defining the bounded pdf g_{Cm} as follows

$$\begin{cases} g_{\mathrm{Cm}}(h; B_{\mathrm{c}}) = f_{\mathrm{Cm}}(h), \ h\sigma < B_{\mathrm{c}} H_{\mathrm{s}} \\ g_{\mathrm{Cm}}(h; B_{\mathrm{c}}) = 1 - F_{\mathrm{Cm}}(h), \ h\sigma = B_{\mathrm{c}} H_{\mathrm{s}} \\ g_{\mathrm{Cm}}(h; B_{\mathrm{c}}) = 0, \ h\sigma > B_{\mathrm{c}} H_{\mathrm{s}} \end{cases} \tag{13}$$

where $B_{\mathrm{c}} > 0$ is the maximum elevation a normalized crest height $C_{\mathrm{m}}/H_{\mathrm{s}}$ may reach. The expectation of the bounded random variable is given by

$$\mathrm{E}\{C_{\mathrm{m}}\}_{\mathrm{BC}} = \sigma \int_0^{\infty} h g_{\mathrm{Cm}} \mathrm{d}h \tag{14}$$

which depends on B_{c} and it is, by construction, smaller than $\mathrm{E}\{C_{\mathrm{m}}\}$, being $\mathrm{E}\{C_{\mathrm{m}}\}_{\mathrm{BC}} = \mathrm{E}\{C_{\mathrm{m}}\}$ in the limit $B_{\mathrm{c}} \to \infty$. Notice that g_{Cm} is a density since

$$\int_0^{\infty} g_{\mathrm{Cm}} \mathrm{d}h = 1 \tag{15}$$

For maximum wave heights H_{m}, we followed a similar strategy by thresholding the values with an upper limit for the crest-to-trough vertical distance $B_{\mathrm{H}} > B_{\mathrm{c}}$, so that the pdf of bounded H_{m} is defined as

$$G_{\mathrm{Hm}}(H; B_{\mathrm{H}}) = f_{\mathrm{Hm}}(H \mid 0 < H_{\mathrm{m}} \leq B_{\mathrm{H}} H_{\mathrm{s}}) \tag{16}$$

and may be written as

$$\begin{cases} G_{\mathrm{Hm}}(H; B_{\mathrm{H}}) = \ f_{\mathrm{Hm}}(H), \ H\sigma < B_{\mathrm{H}} H_{\mathrm{s}} \\ G_{\mathrm{Hm}}(H; B_{\mathrm{H}}) = 1 - F_{\mathrm{Hm}}(H), \ H\sigma = B_{\mathrm{H}} H_{\mathrm{s}} \\ G_{\mathrm{Hm}}(H; B_{\mathrm{H}}) = \ 0, \ H\sigma > B_{\mathrm{H}} H_{\mathrm{s}} \end{cases} \tag{17}$$

The expectation of maximum wave heights H_{m} that are constrained to be below the normalized threshold B_{H} is evaluated as

$$\mathrm{E}\{H_{\mathrm{m}}\}_{\mathrm{BH}} = \ \sigma \int_0^{\infty} H G_{\mathrm{Hm}} \mathrm{d}H \tag{18}$$

and, as anticipated, it is smaller than $\mathrm{E}\{H_{\mathrm{m}}\}$.

In summary, we proposed a modification of the unbounded space-time pdfs of H_{m} and C_{m} by including an upper threshold for both maximum heights that permits a transition of the extreme-value statistics towards zero-probability events. Since in the distribution of extremes the likelihood of having the largest waves above such thresholds increases with the sample size (namely, the number of individual waves N_3, N_2 and N_1), the effect of the bounds is greater when the sea surface area

(or the interval duration) for the characterization of extremes is relatively large. An example of the thresholding effect is shown in Figures 1 and 2, where the bounded and unbounded pdf, cdf, expected values and errors are shown for varying sea surface area width $\sqrt{XY}$. We note that the probability that the threshold values are larger than any wave maximum diminishes with increasing sample size (colored curves from blue to red in Figures 1 and 2). Differences between the bounded and unbounded distributions increase accordingly. With this in mind, in the following sections we focused on the meaningfulness of the threshold and its consequence on the extreme wave prediction over sea states of variable severity.

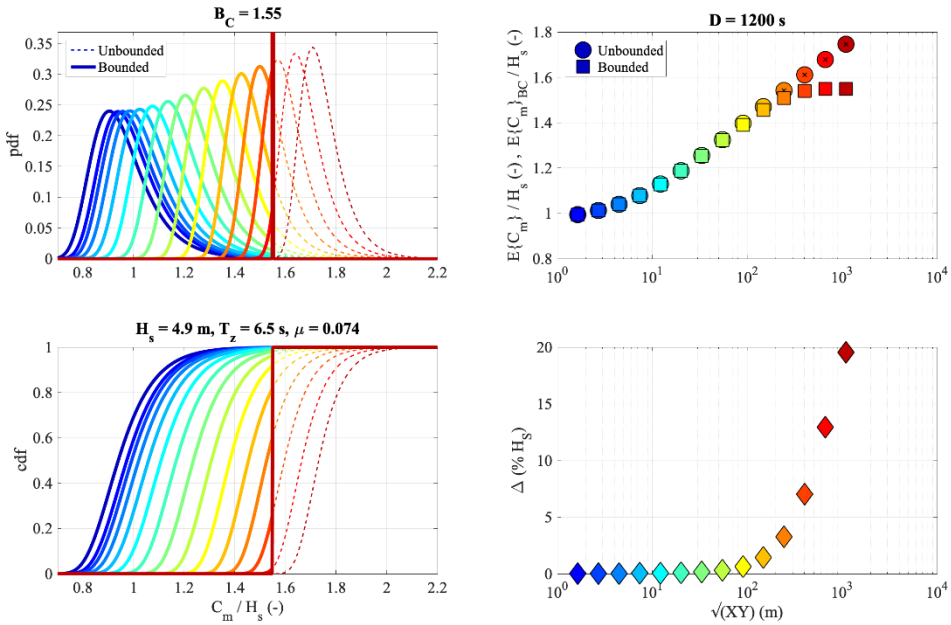

Figure 1. Space-time extreme crest heights C_m. Example of unbounded Gumbel-like distribution and bounded distribution by imposing the upper bound $\max\{C_m\} = 1.55H_s$ ($B_c = 1.55$; see Section 3 for the choice of the threshold value). The temporal interval duration for the extreme assessment is fixed to $D = 1200$ s, whilst the sea surface area XY changes. (top-left) Unbounded (dashed line) and bounded pdf (solid line) color-coded from blue to red with growing sea surface area width $(XY)^{1/2}$ as in the top-right panel. (bottom-left) Unbounded (dashed line) and bounded cdf (solid line) with the same color code as the pdf. (top-right) Variation with $(XY)^{1/2}$ of normalized $E\{C_m\}$ and $E\{C_m\}_{BC}$, and (bottom-right) percentage relative error $\Delta = (E\{C_m\} - E\{C_m\}_{BC})/H_s$. Parameters of the distributions are computed using a directional wave spectrum ($H_s = 4.9$ m; zero-crossing mean spectral period $T_z = 6.5$ s; $\mu = 0.074$) obtained by running the wave model WAVEWATCH III® (see Section 3 for a description of the numerical runs).

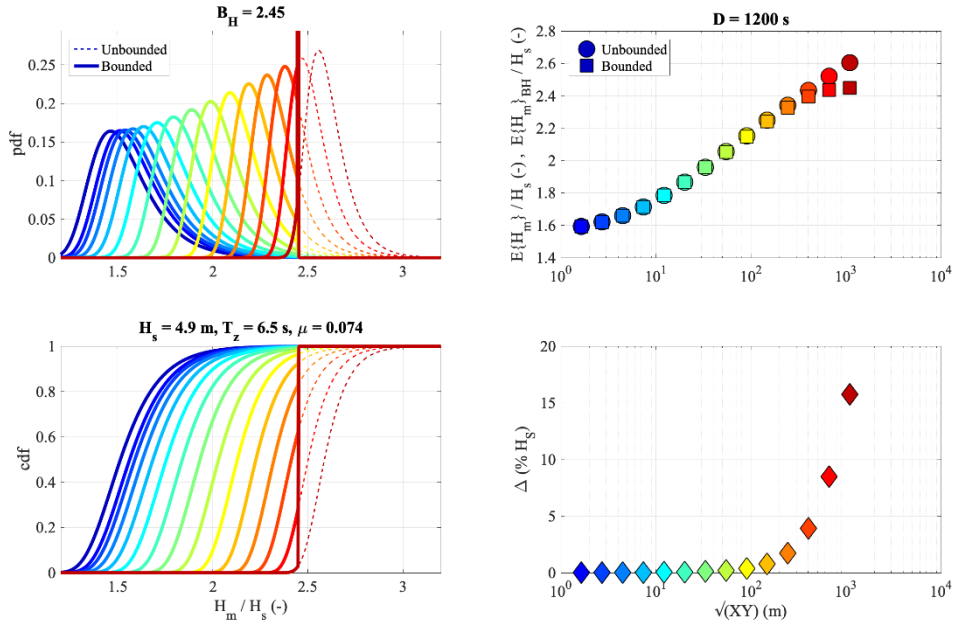

Figure 2. Space-time extreme wave heights H_m. Example of unbounded Gumbel-like distribution and bounded distribution by imposing the upper bound max $\{H_m\} = 2.45H_s$ ($B_H = 2.45$; see Section 3 for the choice of the threshold value). The temporal interval duration for extreme assessment is fixed to $D = 1200$ s, whilst the sea surface area XY changes. (top-left) Unbounded (dashed line) and bounded pdf (solid line) color-coded from blue to red with growing sea surface area width $(XY)^{1/2}$ as in the top-right panel. (bottom-left) Unbounded (dashed line) and bounded cdf (solid line) with the same color code as the pdf. (top-right) Variation with $(XY)^{1/2}$ of normalized $E\{H_m\}$ and $E\{H_m\}_{BH}$, and (bottom-right) percentage relative error $\Delta = (E\{H_m\} - E\{H_m\}_{BH})/H_s$. Parameters of the distributions are computed using a directional wave spectrum ($H_s = 4.9$ m; $T_z = 6.5$ s; $\mu = 0.074$) obtained by running the wave model WAVEWATCH III® (see Section 3 for a description of the numerical runs).

3. Upper Heights and Assessment of the Bounded Distribution

There are not many studies dealing with the ultimate normalized heights C_m/H_s and H_m/H_s that sea waves may reach, since, as we pointed out before, the individual height is not by itself a limiting factor for the wind-wave growth. In the literature, there are a number of credible accounts of giant rogue waves [3], which are among the highest and steepest waves ever recorded in the world's oceans [55,56]. A summary of parameters of some iconic and widely studied rogue waves is reported in Table 1, where individual wave and crest heights are shown after being normalized with the sea severity expressed by the vertical scale H_s, which is the standard way used by scholars and engineers to classify whether a single wave falls within the definition of rogue or not [57]. It is important to mention that the work by Fedele et al. [58] pointed out that rogue wave formation seems to result from constructive interference of elementary waves enhanced by second-order nonlinearities, which is the physical mechanism underlying the theoretical formulations for extremes used in this study.

Table 1. Crest and crest-to-trough maximum wave height parameters of iconic rogue waves (namely Draupner, Andrea, Killard, and El Faro; [6,8]) and of maximum waves AA1 and AA2 gathered within space-time fields of sea elevation [5].

	Draupner	Andrea	Killard	AA1	AA2	El Faro [a]
C_m/H_s (-)	1.55	1.63	1.62	1.59	1.60	1.68
H_m/H_s (-)	2.15	2.49	2.25	-	-	2.60

[a] El Faro values were not derived from observations but obtained from numerical simulations.

For the selected rogue cases, maximum crest heights C_m range between $1.55H_s$ and $1.68H_s$, and maximum wave heights H_m between $2.15H_s$ and $2.60H_s$, the highest values pertaining the rogue event associated to the sinking of the El Faro vessel [6] that were not directly observed but instead obtained from numerical simulations. Moreover, Magnusson and Donelan [59] indicated that the conditions in the Andrea storm were more extreme for steepness and near breaking than in the Draupner case; both individual waves, however, had steepness smaller than the Stokes limit. This suggests that, excluding the very extreme El Faro case that was obtained numerically, likely observed largest values for C_m/H_s and H_m/H_s were in the ranges from 1.55 to 1.65 and from 2.45 to 2.50, respectively, the former limit being also consistent with the values found for space-time maximum elevations (AA1 and AA2 cases in Table 1), and the latter with rogue wave observations off the US West coast [60] for which H_m/H_s peaked at 2.57.

Additionally, it is worth noting, that the two above-mentioned intervals are consistent with each other in the framework of the QD model, supporting the choice of upper bounds that lie within the suggested intervals. Indeed, if we assume for second-order nonlinear crest heights the upper bound $B_C = 1.55$ and the steepness parameter $\mu = 0.06$, the linear threshold for crest height, after [37], equals $1.34H_s$; then, using the wave height bound $B_H = 2.45$, the coefficient $\alpha = \sqrt{2(1-\psi^*)}$ would equal 1.83 and, as a consequence, $\psi^* = -0.67$, which is well within the range from −0.75 to −0.65 of typical values for wind-generated waves [39]. The other way around, assuming $B_H = 2.45$, $\mu = 0.06$, and the mid-value $\psi^* = -0.70$, the upper bound for crest height would be $B_C = 1.54$.

To assess the meaningfulness of the limit B_C for nonlinear crest heights and its impact on the extreme-value distribution, we used the results presented by Fedele et al. [6], who show that the variation with the surface area of the space-time maximum crest heights suggests statistical similarity and universal law (Figure 3). Those authors used a combination of stereo observations (OBS in Figure 3) and Higher-Order pseudo-Spectral numerical simulations (HOS in Figure 3) to assess the growth of space-time maxima (expected values E{·} with subscript ST in Figure 3) over purely temporal maxima (expected values E{·} with subscript T in Figure 3).

Aiming at reproducing the results of Fedele et al. with the unbounded distribution, we have adopted theoretical expectations that were obtained from a sample of one hundred directional wave spectra computed at hourly interval in the Mediterranean Sea, south of the Gulf of Lion (point of coordinates 4.65°E, 42.06°N), using the wave model WAVEWATCH III® (https://polar.ncep.noaa.gov/waves/) forced with ERA5 reanalysis wind fields at 0.25° resolution (https://www.ecmwf.int/en/forecasts/datasets/reanalysis-datasets/era5). The Mediterranean Sea wave model setup is based to cover the whole basin with 0.05° uniform resolution in longitude and latitude and with a spectral grid composed of 36 evenly spaced directions and 32 frequencies exponentially spaced from 0.0500 to 0.9597 Hz at an increment of 10%. WAVEWATCH III® was formulated using the ST4 source term configuration [61], but with adjusted coefficients $\beta_{max} = 1.55$ and $z_{0,max} = 0.002$. To make the analysis reliable, we used a large variety of sea conditions, with the significant wave height H_s ranging between 1.3 and 6.7 m, the mean wavelength L_x between 24 and 85 m, the zero-crossing mean period T_z between 4.4 and 7.9 s, and the mean steepness μ between 0.035 and 0.074. For the extreme-value analysis, the square sea surface region of area XY was considered around the selected point.

We observe in Figure 3 that normalized values of unbounded E{C_m} and bounded E{C_m}$_{BC}$ extreme-value crest heights tend to part when $\sqrt{XY}$ is above ~$2L_x$, and the maximum difference between E{C_m}$_{BC}$ and El Faro HOS simulations is about +6% (+9%) of the mean temporal maximum when the limiting threshold $B_c = 1.55$ ($B_c = 1.60$) is adopted. Then, over larger areas, the differences between numerical outputs and theoretical expectations E{C_m}$_{BC}$ reduce, and they tend to reconcile for width $\sqrt{XY} >$ ~$20L_x$ by setting $B_c = 1.55$. The use of a higher limit such as $B_c = 1.60$ seems to produce a poorer matching against HOS numerical outputs, at least within the spatial range for which they are available (blue line in Figure 3). In conclusion, we first acknowledge that a universal law for space-time wave extremes is not yet fully validated and needs further understanding. Nevertheless, these results show that the use of an upper bounded distribution (green markers in Figure 3) both reduces the

overestimation over large areas of space time maximum crest heights and produces a more realistic saturation of surface heights in comparison to an unbounded distribution (red markers in Figure 3).

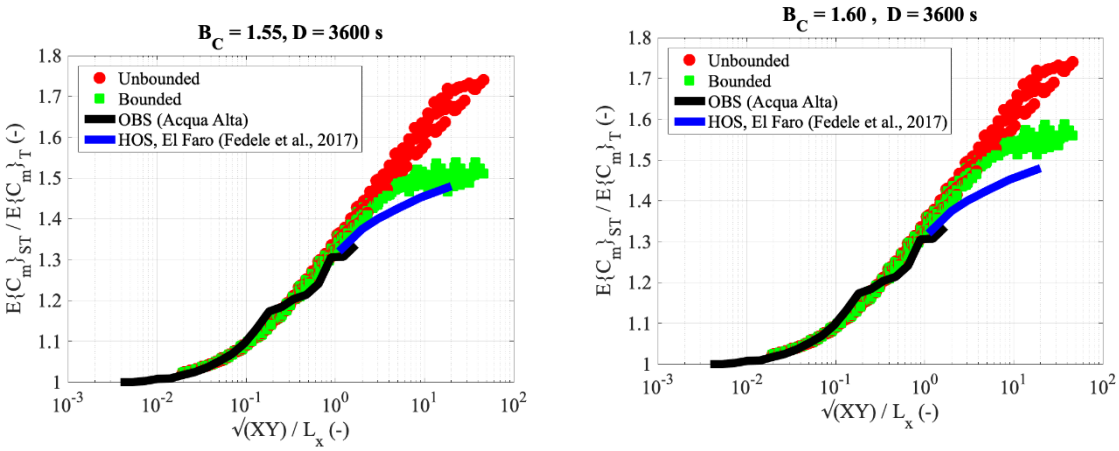

Figure 3. Assessment of the space-time extreme bounded distribution of C_m. Theoretical ratio between space-time (ST) and time (T) extreme expectations as a function of the normalized sea surface area width $(XY)^{1/2}/L_X$ (L_X is the spectral mean wavelength) for the unbounded (red markers) and the bounded distribution (green markers). The time-interval duration is D = 3600 s, as in Fedele et al. [6]. OBS: stereo observations from the Acqua Alta oceanographic platform (Adriatic Sea, Italy, [62]); HOS: Higher-Order pseudo-Spectral numerical simulations (adapted from [6]). (**left**) Upper bound B_C = 1.55, and (**right**) upper bound B_C = 1.60.

4. Impact of the Upper Bounds on Space-Time Extreme Waves

The impact of the upper bound on space-time extreme waves was examined by evaluating the theoretical difference between the expected values of the unbounded and bounded maximum heights when the sea state characteristics and sea surface areas were varied. Expected maximum crest and wave heights were obtained via numerical integration of the corresponding pdf. We considered two time intervals: D = 1200 s, which is the wave buoy record standard length that has been used in previous assessments of space-time extremes from model data [33], and D = 3600 s, which is the generally accepted maximum time interval for a sea state to be considered stationary [63]. We assume the two upper limits B_c = 1.55 and B_H = 2.45, and we vary the area width $\sqrt{XY}$ by keeping $X = Y$. Results are presented, at first, by assessing the error (i.e., overestimation) committed in using the unbounded distribution as a function of the unbounded expected heights; then, we considered how this error changes with the area size and the sea severity. Theoretical results were obtained using the same set of directional spectra as in the previous section.

Figure 4 shows that the overestimation increases with increasing extreme height values $E\{C_m\}/H_s$ and $E\{H_m\}/H_s$. When the normalized expected values of the unbounded pdf equal the two thresholds B_c = 1.55 and B_H = 2.45, the difference (unbounded - bounded) is however smaller than +4% of H_s, while for higher values the errors tend to cluster around a steady growth. The two time intervals produce different results (the shorter one, 1200 s, allows for smaller errors), but for both cases these errors remain quite small below the threshold (<+4%). Since the expected values of extremes depend on the sea severity (i.e., H_s) of the sea state [64], overestimations do vary with H_s, as is shown in Figures 5 and 6, which provide the relative errors $\Delta(C_m) = (E\{C_m\} - E\{C_m\}_{BC})/H_s$ and $\Delta(H_m) = (E\{H_m\} - E\{H_m\}_{BH})/H_s$ as a function of H_s, $\sqrt{XY}$, and D. For both interval durations, errors are smaller for more energetic sea states (i.e., large H_s) and grow with the sea surface area (i.e., sample size). Moreover, in order to keep errors as low as 5% of H_s for the more severe sea conditions, area sides must remain smaller than about 300 m.

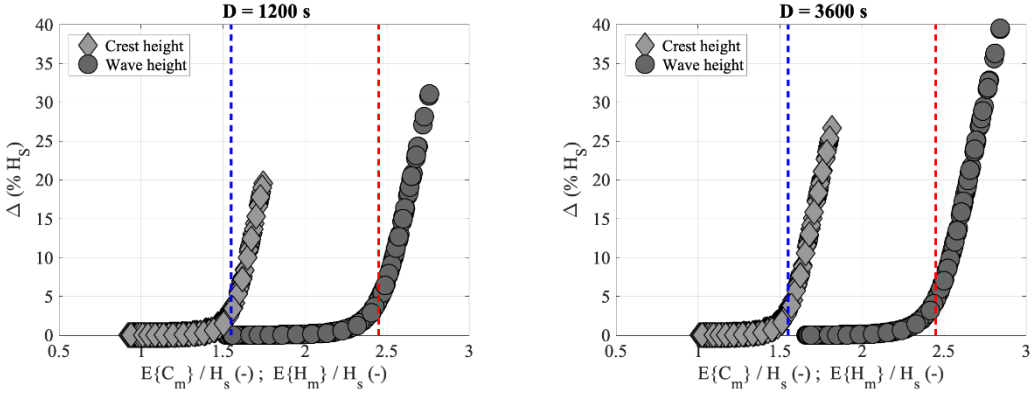

Figure 4. Space-time extreme crest and wave heights. Relative errors Δ given by $(\mathrm{E}\{C_m\} - \mathrm{E}\{C_m\}_{BC})/H_s$ and $(\mathrm{E}\{H_m\} - \mathrm{E}\{H_m\}_{BH})/H_s$ as a function of the normalized expectations $\mathrm{E}\{C_m\}/H_s$ and $\mathrm{E}\{H_m\}/H_s$, respectively. The vertical lines show the two ultimate dimensionless heights $B_C = 1.55$ (dashed blue line) and $B_H = 2.45$ (dashed red line). (**left**) Time interval duration $D = 1200$ s and (**right**) time interval duration $D = 3600$ s. Sea state parameters: H_s between 1.3 and 6.7 m, mean wavelength L_x between 24 and 85 m, zero-crossing mean period T_z between 4.4 and 7.9 s, and mean steepness μbetween 0.035 and 0.074.

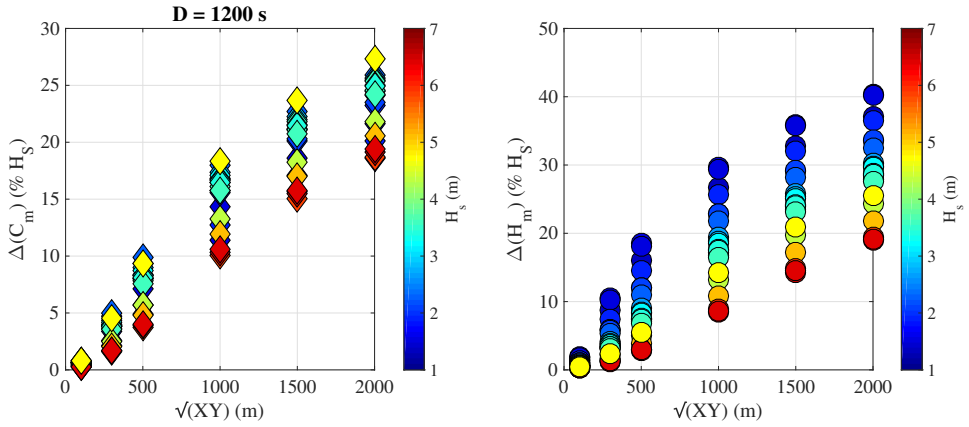

Figure 5. Space-time extreme crest and wave heights. Relative errors $\Delta(C_m) = (\mathrm{E}\{C_m\} - \mathrm{E}\{C_m\}_{BC})/H_s$ (**left**), and $\Delta(H_m) = (\mathrm{E}\{H_m\} - \mathrm{E}\{H_m\}_{BH})/H_s$ (**right**) as a function of the sea surface area width. Upper limit $B_C = 1.55$ and $B_H = 2.45$. Markers are color-coded with the value of the significant wave height H_s of each directional spectrum. Time interval duration $D = 1200$ s.

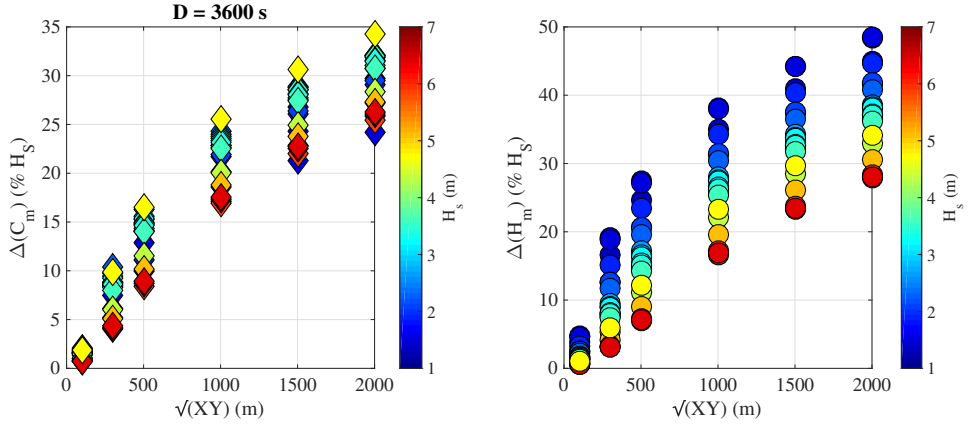

Figure 6. Space-time extreme crest and wave heights. Relative errors $\Delta(C_m) = (\mathrm{E}\{C_m\} - \mathrm{E}\{C_m\}_{BC})/H_s$ (**left**), and $\Delta(H_m) = (\mathrm{E}\{H_m\} - \mathrm{E}\{H_m\}_{BH})/H_s$ (**right**) as a function of the sea surface area width. Upper limit $B_C = 1.55$ and $B_H = 2.45$. Markers are color-coded with the value of the significant wave height H_s of each directional spectrum. Time interval duration $D = 3600$ s.

5. Concluding Remarks

In this study we have proposed and tested an improvement of the extreme-value pdf of space-time maximum waves in order to include an upper bound for nonlinear crest heights and crest-to-trough wave heights. Indeed, the pdf of unbounded extremes, being based on Gaussianity, has no physical limits on the maximum values that the surface height or crest-to-trough height could attain. This poses a limitation on the probability functions based on asymptotic expansion, which require large heights in order to be effective. A practical trade-off was suggested in this study. The solution was based on a thresholded Gumbel-like distribution of short-term/range space-time extreme waves, but its general approach might be applied to time extreme waves as well. Fundamental in the thresholding is the selection of the upper bounds that we have fixed as a multiple of the significant wave height, stemming from the highest values reached by rogue waves. A preliminary assessment of the bounded pdf was made using reference values from previous research studies. Finally, the overestimation induced by the unbounded pdf over large areas was evaluated. Main conclusions of the study may be summarized as follows:

- The extreme-value bounded distribution alleviates the overestimation of the unbounded distribution over large areas. The use of limiting heights allows a smooth transition towards a realistic saturation of crest and wave heights with increasing sample size. Although the proposed pdf used a simplified measure of the limit for wave growth, it improves the performance of the space-time extreme pdf, while leaving its skill for small areas unchanged.
- Primary in the proper assessment of the bounded pdf is the definition of the upper limits. Here we have used $1.55H_s$ and $2.45H_s$ for the maximum crest and wave heights, respectively, which were derived from historical rogue wave parameters. However, more validation studies are needed to improve the knowledge on the confidence limits for varying sea state characteristics. Numerical studies, using for instance HOS simulations, seem to be promising for this purpose, allowing for investigation of nonlinear wave groups crossing sea surface regions with a different area.
- Our analysis has shown that the unbounded pdfs are reliable over surface areas with a side smaller than $O(10^2$ m) for all sea states and time interval shorter than one hour. More energetic (and potentially damaging) sea conditions however are less influenced by the inclusion of the bounds, since, for a given area, they provide smaller sample sizes.
- The proposed formulations are suitable for being integrated into phase-averaged spectral wave models to expand their range of applicability for a proper characterization of extreme wave parameters.

Author Contributions: A.B.: conceptualization, methodology, formal analysis, supervision, writing—original draft, project administration, funding acquisition; F.B.: software, investigation; S.D.: software, investigation. All authors have read and agreed to the published version of the manuscript.

Funding: This work has been partially carried out as part of the Copernicus Marine Environment Monitoring Service (CMEMS) LATEMAR project. CMEMS is implemented by Mercator Ocean in the framework of a delegation agreement with the European Union.

Acknowledgments: We are grateful to Luigi Cavaleri (CNR-ISMAR) for useful discussions on wave models, and Marco Marani (University of Padua) for insights on the extreme-value statistics.

Conflicts of Interest: The authors declare that there is no competition financial interests or personal relationships that could appear to influence the work reported in this paper.

References

1. Onorato, M.; Osborne, A.; Serio, M.; Bertone, S. Freak Waves in Random Oceanic Sea States. *Phys. Rev. Lett.* **2001**, *86*, 5831–5834. [CrossRef] [PubMed]
2. Janssen, P.A.E.M. Nonlinear Four-Wave Interactions and Freak Waves. *J. Phys. Oceanogr.* **2003**, *33*, 863–884. [CrossRef]
3. Dysthe, K.; Krogstad, H.E.; Müller, P. Oceanic Rogue Waves. *Annu. Rev. Fluid Mech.* **2008**, *40*, 287–310. [CrossRef]

4. Gemmrich, J.; Garrett, C. Dynamical and statistical explanations of observed occurrence rates of rogue waves. *Nat. Hazards Earth Syst. Sci.* **2011**, *11*, 1437–1446. [CrossRef]
5. Benetazzo, A.; Ardhuin, F.; Bergamasco, F.; Cavaleri, L.; Veras, P.; Schwendeman, M.; Sclavo, M.; Thomson, J.; Torsello, A.; Guimarães, P.V.; et al. On the shape and likelihood of oceanic rogue waves. *Sci. Rep.* **2017**, *7*, 1–11. [CrossRef]
6. Fedele, F.; Lugni, C.; Chawla, A. The sinking of the El Faro: Predicting real world rogue waves during Hurricane Joaquin. *Sci. Rep.* **2017**, *7*, 1–15. [CrossRef]
7. Cavaleri, L.; Bertotti, L.; Torrisi, L.; Bitner-Gregersen, E.; Serio, M.; Onorato, M. Rogue waves in crossing seas: The Louis Majesty accident. *J. Geophys. Res. Ocean.* **2012**, *117*, 1–8. [CrossRef]
8. Donelan, M.A.; Magnusson, A.-K. The Making of the Andrea Wave and other Rogues. *Sci. Rep.* **2017**, *7*, 44124. [CrossRef]
9. Cavaleri, L.; Barbariol, F.; Benetazzo, A.; Bertotti, L.; Bidlot, J.-R.; Janssen, P.; Wedi, N. The Draupner wave: A fresh look and the emerging view. *J. Geophys. Res. Ocean.* **2016**, *121*, 6061–6075. [CrossRef]
10. Slunyaev, A.; Pelinovsky, E.; Guedes Soares, C. Modeling freak waves from the North Sea. *Appl. Ocean Res.* **2005**, *27*, 12–22. [CrossRef]
11. Onorato, M.; Residori, S.; Bortolozzo, U.; Montina, A.; Arecchi, F.T. Rogue waves and their generating mechanisms in different physical contexts. *Phys. Rep.* **2013**, *528*, 47–89. [CrossRef]
12. Waseda, T.; Hallerstig, M.; Ozaki, K.; Tomita, H. Enhanced freak wave occurrence with narrow directional spectrum in the North Sea. *Geophys. Res. Lett.* **2011**, *38*. [CrossRef]
13. Dematteis, G.; Grafke, T.; Onorato, M.; Vanden-Eijnden, E. Experimental Evidence of Hydrodynamic Instantons: The Universal Route to Rogue Waves. *Phys. Rev. X* **2019**, *9*, 041057. [CrossRef]
14. Toffoli, A.; Lefèvre, J.M.; Bitner-Gregersen, E.; Monbaliu, J. Towards the identification of warning criteria: Analysis of a ship accident database. *Appl. Ocean Res.* **2005**, *27*, 281–291. [CrossRef]
15. Bitner-Gregersen, E.M.; Gramstad, O. ROGUE WAVES. Impact on Ships and Offshore Structures. DNV GL STRATEGIC RESEARCH & INNOVATION POSITION PAPER 05–2015. 2015. Available online: https://issuu.com/dnvgl/docs/rogue_waves_final (accessed on 3 September 2020).
16. Didenkulova, E. Catalogue of rogue waves occurred in the World Ocean from 2011 to 2018 reported by mass media sources. *Ocean Coast. Manag.* **2020**, *188*, 105076. [CrossRef]
17. Barbariol, F.; Alves, J.H.G.; Benetazzo, A.; Bergamasco, F.; Bertotti, L.; Carniel, S.; Cavaleri, L.; Chao, Y.Y.; Chawla, A.; Ricchi, A.; et al. Numerical Modeling of Space-Time Wave Extremes using WAVEWATCH III. *Ocean Dyn.* **2017**, *67*, 535–549. [CrossRef]
18. ECMWF IFS DOCUMENTATION–Cy46r1 Operational Implementation 6 June 2019 PART VII: ECMWF WAVE MODEL. 2019. Available online: https://www.ecmwf.int/en/elibrary/19311-part-vii-ecmwf-wave-model (accessed on 3 September 2020).
19. Barbariol, F.; Benetazzo, A.; Carniel, S.; Sclavo, M. Space–Time Wave Extremes: The Role of Metocean Forcings. *J. Phys. Oceanogr.* **2015**, *45*, 1897–1916. [CrossRef]
20. Sclavo, M.; Barbariol, F.; Bergamasco, F.; Carniel, S.; Benetazzo, A. Italian seas wave extremes: A preliminary assessment. *Rend. Lincei* **2015**, *26*, 25–35. [CrossRef]
21. Longuet-Higgins, M.S. On the statistical distribution of the heights of sea waves. *J. Mar. Res.* **1952**, *11*, 245–265.
22. Mori, N.; Janssen, P.A.E.M. On Kurtosis and Occurrence Probability of Freak Waves. *J. Phys. Oceanogr.* **2006**, *36*, 1471–1483. [CrossRef]
23. Fedele, F.; Tayfun, M.A. On nonlinear wave groups and crest statistics. *J. Fluid Mech.* **2009**, *620*, 221–239. [CrossRef]
24. Adler, R.J. *The Geometry of Random Fields*; John Wiley: New York, NY, USA, 1981; p. 302.
25. Piterbarg, V.I. *Asymptotic Methods in the Theory of Gaussian Processes and Fields*; Translations of Mathematical Monographs; American Mathematical Society: Providence, RI, USA, 1996; p. 206.
26. Fedele, F. Space–Time Extremes in Short-Crested Storm Seas. *J. Phys. Oceanogr.* **2012**, *42*, 1601–1615. [CrossRef]
27. Krogstad, H.E.; Liu, J.; Socquet-Juglard, H.; Dysthe, K.; Trulsen, K. Spatial Extreme Value Analysis of Nonlinear Simulations of Random Surface Waves. In Proceedings of the OMAE04 23rd International Conference on Offshore Mechanics and Arctic Engineering, Vancouver, BC, Canada, 20–25 June 2004; pp. 285–295.

28. Fedele, F.; Benetazzo, A.; Gallego, G.; Shih, P.-C.; Yezzi, A.; Barbariol, F.; Ardhuin, F. Space–time measurements of oceanic sea states. *Ocean Model.* **2013**, *70*, 103–115. [CrossRef]
29. Baxevani, A.; Rychlik, I. Maxima for Gaussian seas. *Ocean Eng.* **2004**, *33*, 895–911. [CrossRef]
30. Fedele, F. On certain properties of the compact Zakharov equation. *J. Fluid Mech.* **2014**, *748*, 692–711. [CrossRef]
31. Babanin, A. *Breaking and Dissipation of Ocean Surface Waves*; Cambridge University Press: Cambridge, UK, 2011; ISBN 9780511736162.
32. Benetazzo, A.; Barbariol, F.; Bergamasco, F.; Torsello, A.; Carniel, S.; Sclavo, M. Observation of extreme sea waves in a space-time ensemble. *J. Phys. Oceanogr.* **2015**, *45*, 2261–2275. [CrossRef]
33. Barbariol, F.; Bidlot, J.-R.; Cavaleri, L.; Sclavo, M.; Thomson, J.; Benetazzo, A. Maximum wave heights from global model reanalysis. *Prog. Oceanogr.* **2019**, *175*, 139–160. [CrossRef]
34. Mendes, S.; Scotti, A. Rogue wave statistics in (2+1) Gaussian seas I: Narrow-banded distribution. *Appl. Ocean Res.* **2020**, *99*, 102043. [CrossRef]
35. Fedele, F.; Gallego, G.; Yezzi, A.; Benetazzo, A.; Cavaleri, L.; Sclavo, M.; Bastianini, M. Euler characteristics of oceanic sea states. *Math. Comput. Simul.* **2012**, *82*, 1102–1111. [CrossRef]
36. Benetazzo, A.; Barbariol, F.; Pezzutto, P.; Staneva, J.; Behrens, A.; Davison, S.; Bergamasco, F.; Sclavo, M.; Cavaleri, L. Towards a unified framework for extreme sea waves from spectral models: Rationale and applications. *Ocean Eng.* **2020**, under review.
37. Tayfun, M.A. Narrow-band nonlinear sea waves. *J. Geophys. Res.* **1980**, *85*, 1548–1552. [CrossRef]
38. Benetazzo, A.; Barbariol, F.; Bergamasco, F.; Sandro, C.; Sclavo, M.; Yoo, J.; Cavaleri, L.; Kim, S.S.; Bertotti, L.; Barbariol, F.; et al. Space-time extreme wind waves: Analysis and prediction of shape and height. *Ocean Model.* **2017**, *113*, 201–216.
39. Boccotti, P. *Wave Mechanics for Ocean Engineering*; Elsevier Science B.V.: Amsterdam, The Netherlands, 2000; Volume 64, p. 496.
40. Adler, R.J. On excursion sets, tube formulas and maxima of random fields. *Ann. Appl. Probab.* **2000**, *10*, 1–74. [CrossRef]
41. Naess, A. On the distribution of crest to trough wave heights. *Ocean Eng.* **1985**, *12*, 221–234. [CrossRef]
42. Liu, P.C.; Babanin, A.V. Using wavelet spectrum analysis to resolve breaking events in the wind wave time series. *Ann. Geophys.* **2004**, *22*, 3335–3345. [CrossRef]
43. Bonmarin, P. Geometric properties of deep-water breaking waves. *J. Fluid Mech.* **1989**, *209*, 405–433. [CrossRef]
44. Stokes, G.G. Considerations Relative to the Greatest Height of Oscillatory Irrotational Waves Which Can Be Propagated without Change of Form. In *On the Theory of Oscillatory Waves*; Cambridge University Press: London, UK, 1880; pp. 225–229.
45. Brown, M.G.; Jensen, A. Experiments on focusing unidirectional water waves. *J. Geophys. Res. Ocean.* **2001**, *106*, 16917–16928. [CrossRef]
46. Babanin, A.; Chalikov, D.; Young, I.; Savelyev, I. Predicting the breaking onset of surface water waves. *Geophys. Res. Lett.* **2007**, *34*, L07605. [CrossRef]
47. Babanin, A.V.; Chalikov, D.; Young, I.R.; Savelyev, I. Numerical and laboratory investigation of breaking of steep two-dimensional waves in deep water. *J. Fluid Mech.* **2010**, *644*, 433–463. [CrossRef]
48. Manolidis, M.; Orzech, M.; Simeonov, J. Rogue Wave Formation in Adverse Ocean Current Gradients. *J. Mar. Sci. Eng.* **2019**, *7*, 26. [CrossRef]
49. Tayfun, M.A. Distributions of envelope and phase in wind waves. *J. Phys. Oceanogr.* **2008**, *38*, 2784–2800. [CrossRef]
50. Rapp, R.J.; Melville, W.K. Laboratory measurements of deep-water breaking waves. *Philos. Trans. R. Soc. Lond. Ser. A Math. Phys. Sci.* **1990**, *331*, 735–800.
51. Holthuijsen, L.H.; Herbers, T.H.C. Statistics of Breaking Waves Observed as Whitecaps in the Open Sea. *J. Phys. Oceanogr.* **1986**, *16*, 290–297. [CrossRef]
52. Schwendeman, M.; Thomson, J. Sharp-crested Breaking Surface Waves Observed from a Ship-Based Stereo Video System. *J. Phys. Oceanogr.* **2017**, *47*, 775–792. [CrossRef]
53. Banner, M.L.; Babanin, A.V.; Young, I.R. Breaking Probability for Dominant Waves on the Sea Surface. *J. Phys. Oceanogr.* **2000**, *30*, 3145–3160. [CrossRef]

54. Filipot, J.-F.; Ardhuin, F.; Babanin, A.V. A unified deep-to-shallow water wave-breaking probability parameterization. *J. Geophys. Res.* **2010**, *115*, C04022. [CrossRef]
55. Liu, P.C. A chronology of freaque wave encounters. *Geofizika* **2007**, *24*, 57–70.
56. Kharif, C.; Pelinovsky, E.; Slunyaev, A. *Rogue Waves in the Ocean*; Springer: Berlin, Germany, 2009; p. 216, ISBN 9783540884187.
57. Draper, L. 'Freak' ocean waves. *Mar. Obs.* **1965**, *35*, 193–195. [CrossRef]
58. Fedele, F.; Brennan, J.; de León, S.P.; Dudley, J.; Dias, F. Real world ocean rogue waves explained without the modulational instability. *Sci. Rep.* **2016**, *6*, 1–11. [CrossRef]
59. Magnusson, A.K.; Donelan, M.A. The Andrea Wave Characteristics of a Measured North Sea Rogue Wave. *J. Offshore Mech. Arct. Eng.* **2013**, *135*, 1–10. [CrossRef]
60. Baschek, B.; Imai, J. Rogue Wave Observations off the US West Coast. *Oceanography* **2011**, *24*, 158–165. [CrossRef]
61. Ardhuin, F.; Rogers, E.; Babanin, A.; Filipot, J.-F.; Magne, R.; Roland, A.; Van Der Westhuysen, A.; Queffeulou, P.; Lefevre, J.-M.; Aouf, L.; et al. Semi-empirical dissipation source functions for ocean waves: Part I, definition, calibration and validation. *J. Phys. Oceanogr.* **2010**, *40*, 1917–1941. [CrossRef]
62. Benetazzo, A.; Fedele, F.; Gallego, G.; Shih, P.-C.; Yezzi, A. Offshore stereo measurements of gravity waves. *Coast. Eng.* **2012**, *64*, 127–138. [CrossRef]
63. Holthuijsen, L.H. *Waves in Oceanic and Coastal Waters*; Cambridge University Press: Cambridge, UK, 2007; p. 387.
64. Ochi, M.K. *Ocean Waves*; Cambridge University Press: Cambridge, UK, 1998; ISBN 9780521563789.